Precise measurement of the rotational Raman gain coefficient in para-hydrogen by the large-signal method

Akira Tsunemi, Keigo Nagasaka, and Hideo Tashiro

The plane-wave gain coefficient of stimulated rotational Raman scattering in para-H_2 was determined for CO_2 laser-pumping pulses. Difficulties caused by lowered substantial gain for stimulated scattering in the infrared region were overcome by measuring converted energies instead of powers in the large-signal region. The measured gain coefficients showed excellent agreement with theoretical values.

Key words: Stimulated rotational Raman scattering, plane-wave gain coefficient, parahydrogen, large-signal method.

I. Introduction

For parahydrogen Raman lasers,[1–5] there has been a critical difference between gain values estimated theoretically and those obtained experimentally. Compared with theoretical coefficients, the coefficients estimated through experiments of the para-H_2 Raman laser[6,7] were smaller by a factor of 0.7. Such disagreement causes a crucial problem in the optimal designing of the apparatus, especially for scaling up the laser system. Apart from the practical importance of this disagreement, generally it is worth verifying the validity of the polarizability theory[8] to the cases that are pumped with infrared radiation.

The Raman gain coefficient for CO_2 laser pumping has been estimated, in a usual manner, from the growth rate in the small-signal region.[6,7] To overcome its low effective gain, the para-H_2 Raman laser requires a multiple-pass cell (MPC),[9] which provides a long interaction length with repeated focusing. However, the beam-crossing effect[10] caused by the beam trajectory in a MPC makes it ambiguous to evaluate the gain coefficient, because the precise evaluation of the interaction length becomes difficult under such beam-crossing configuration. Corat *et al.*[11] claimed that the gain coefficient measured in a MPC agreed well with the theoretical one. However, in their analysis, the contributions of the beam-crossing effect and the transient response of the stimulated rotational Raman scattering (SRRS) were not considered. Transient effects[12,13] are critical and cannot be neglected because the delay of the peak of a Stokes pulse from the pump pulse is observed clearly, although the dephasing time of the medium is much smaller than the width of a pump pulse.

To measure the gain coefficient precisely in the infrared stimulated Raman scattering (SRS), we proposed and carried out a reliable method that utilized a single-pass cell. The principle of this method is described in Section II. Section III presents an experimental setup for the measurements. In Section IV we present the experimental results. In Section V we discuss the accuracy of the measurement and the cause of the disagreement of the experimental values reported previously in the literature.

II. Principle of Measurement

To exclude uncertainty caused by a beam-intersection effect in a MPC, we chose a cell with only a single transit for the measurement. However, because of a low Raman gain for infrared frequencies, a single transit cannot produce a power gain that is large enough to be measured. In addition, under such a low growth of the Stokes wave, it is difficult to monitor the precise temporal profiles of pulses for the discussion of transient effect. However, in the large-signal limit where the power of the Stokes wave depletes the pump power, the converted Stokes energy becomes measurable, even with a single-pass

Akira Tsunemi and Keigo Nagasaka are with the Department of Physics, Science University of Tokyo, Kagurazaka 1-3, Shinjuku-ku, Tokyo 162, Japan. Hideo Tashiro is with Riken, The Institute of Physical and Chemical Research, Horosawa 2-1, Wako-shi, Saitama 351-01, Japan.

Received 6, August 1991.
0003-6935/92/214165-07$05.00/0.

cell. Additional merits of the single-transit measurement in the large-signal region are as follows: (1) because powers of both waves are comparable, the probe Stokes component is separated easily and filtered from the pump wave compared with that for the measurement in the small-signal region; (2) temporal and spatial overlapping of the generated pump and Stokes beams are well defined; and (3) no dynamic range as wide as that required in the measurements for the small-signal region is needed for detectors.

Analysis of the experimental data, however, becomes somewhat complicated and is helped by a numerical calculation. For the analysis of transient SRS, we utilize three differential equations that describe the pump and Stokes fields and the molecular vibration or rotation of the Raman medium that is coupled with the nonlinear polarization.[14] Conversion between the pump and Stokes powers and the vibration amplitude of the Raman medium are described by the following equations.

$$\frac{dP_p}{dZ} = -\frac{\omega_p}{\omega_s} AV\sqrt{P_p P_s}\left\{\frac{2}{\pi[W_p(z)^2 + W_s(z)^2]}\right\}^{1/2}. \tag{1a}$$

$$\frac{dP_s}{dZ} = AV\sqrt{P_p P_s}\left\{\frac{2}{\pi[W_p(z)^2 + W_s(z)^2]}\right\}^{1/2}, \tag{1b}$$

$$\frac{dV}{dt} = B\sqrt{P_p P_s}\left\{\frac{2}{\pi[W_p(z)^2 + W_s(z)^2]}\right\}^{1/2} - \frac{\Gamma}{2}V, \tag{1c}$$

where P_p and P_s indicate the pump and Stokes powers, respectively; the strength of the medium vibration is described as V; and ω_p and ω_s are the angular frequencies of the pump and Stokes waves, respectively. The spot sizes of pump and Stokes beams are written as $W_p(z)$ and $W_s(z)$, respectively; Γ indicates the dephasing constant of the medium; and A and B are the constants related to the differential cross section of the SRRS. The plane-wave Raman gain coefficient g is expressed as

$$g = \frac{2AB}{\Gamma}. \tag{2}$$

A detailed explanation and derivation of the equations are given in Appendix A. The gain coefficient of the SRRS in para-H_2 is finally determined by fitting increased Stokes energies, which are acquired by comparing pulse profiles obtained by simulation with those obtained by experiment.

In practice, the application of the above numerical analysis requires the following procedure. First, powers of both pump and Stokes pulses should be well suited to the single-pass cell to gain the sufficient SRRS interaction. Second, the temporal profiles of the pump and Stokes pulses are monitored at both the entrance and the exit of the cell. The signals are digitized and stored into the memory to compare with the calculation. Third, pulse energies are measured by energy meters at the same time. The absolute powers of pulses, $P_{pi}(t)$, $P_{si}(t)$, $P_{po}(t)$ and $P_{so}(t)$, are then calibrated. Fourth, the amount of converted energies is estimated. The increment of Stokes energy, ΔE_s, is obtained by integrating $P_{si}(t)$ and $P_{so}(t)$:

$$\Delta E_s = \int P_{so}(t) - P_{si}(t)\mathrm{d}t. \tag{3}$$

Fifth, the SRS is simulated by using the coupled equations with the gain coefficient g as a fitting parameter. The increase of the Stokes energy $\Delta E_s'$ is also estimated from $P_{so}(t)'$ in the same manner as ΔE_s. Then we introduce the function that indicates the difference between $\Delta E_s'$ and ΔE_s:

$$D(g) = |\Delta E_s' - \Delta E_s| = 0. \tag{4}$$

The final gain coefficient g_0 is the value that makes $D(g_0) = 0$.

In practical calculations, we used the finite-differential method in which dz and dt were set to be 1 cm and 1/30 ns, respectively. For the determination of the Raman gain coefficient, we continued the computer calculation until a calculated value of $\Delta E_s'$ agreed with ΔE_s up to five figures.

III. Experimental Setup

The experimental setup is shown in Fig. 1. A pump pulse was generated by a single-mode transversely excited atmospheric (TEA)–CO_2 laser oscillator with a low-pressure gain cell and was amplified by a two-stage TEA–CO_2 amplifier. The lasing line was tuned to $10R(30)$. A pump pulse presented as (a) in Fig. 1 was introduced to the MPC filled with 1400 Torr of para-H_2 at room temperature. In this condition, the Stokes pulse with its pump pulse came out of the MPC, as shown in (b) in Fig. 1. The pump pulse showed a slight decrement of the power in accordance with Raman conversion to the Stokes pulse. To produce Stokes pulses that are suited to the following ΔE_s measurement in a single-pass cell, we carefully adjusted the CO_2 laser power by controlling a discharge voltage of the TEA–CO_2 amplifiers. Output pulses from the MPC were already well collimated and synchronized. These characteristics are essential for the precise measurement of the gain coefficient. Before the two coupled pulses were introduced to the single-pass cell, a few percentages of pump and Stokes powers were split by KCl and led to photon drag detectors independently. A BaF_2 filter was inserted on the way to the detector for pump pulses. For the detection of Stokes pulse profiles, we attenuated pump powers by the reststrahlen reflection of laser-induced fluorescence plates.

The single-pass cell had a length of 4 m and was also operated at room temperature. The pressure of para-H_2 was varied between 130 and 3040 Torr. The incident-laser beams were focused at the center of the cell. The spatial-beam profiles were measured at both the entrance and the exit of the cell. Focusing points and beam-waist sizes of the pump and Stokes beams were estimated, respectively, by using the following equation[15]:

$$W_{(z)}^2 = W_0^2\left[1 + \left(\frac{\lambda z}{\pi W_0^2}\right)^2\right]. \tag{5}$$

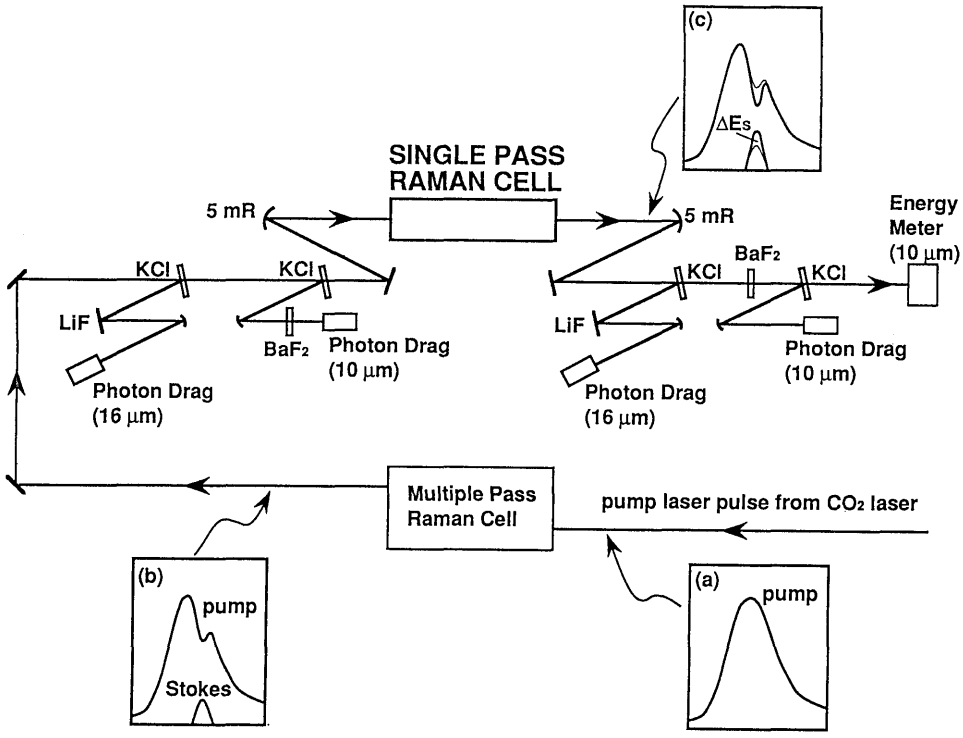

Fig. 1. Experimental setup. The multiple-pass Raman cell was used as a Stokes generator. Typical pulse shapes at three points are indicated as inserts (a), (b), and (c).

The averaged profile of a pump pulse measured at the entrance is shown in Fig. 2. The dashed curve is a Gaussian curve fitted by the least-squares method. The curve traces the experimental points excellently. Excellent agreement with Gaussians curve was also obtained for the pump pulse at the exit and Stokes pulses at both the entrance and the exit of the cell. In numerical calculation, therefore, beam profiles of both the pump and Stokes beams were ensured to be in the TEM_{00} mode. This well-defined beam feature is an additional advantage that is acquired by the use of an MPC as a Stokes generator. It is known that the MPC can exclude higher-order spatial modes and then transmits only the TEM_{00} mode, because of its resonator structure and long total pass length.[16,17] After the transit of the single-pass cell, the beams were corrected to a parallel beam by a mirror that was 5 m in curvature. The temporal pulse profiles were then detected by photon drag detectors and were compared with those at the entrance.

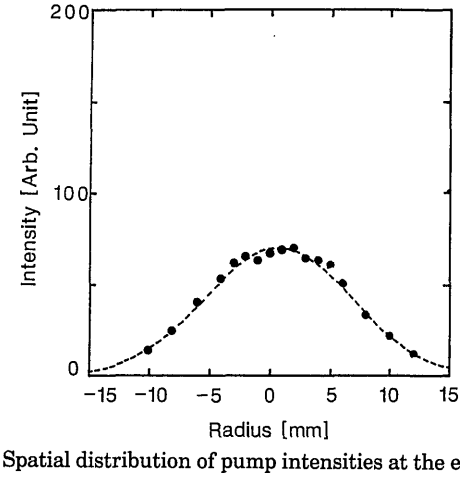

Fig. 2. Spatial distribution of pump intensities at the entrance of the single-pass Raman cell. The fitted Gaussian curve is shown with a dashed curve.

The calibration of powers were made as follows. In general, calibration factors C_p and C_s for pump and Stokes pulses, respectively, were obtained from the measured temporal profiles and energies. For simplification, instead of measuring energies of four related pulses at the same time, we measured only the pump energy at the exit of the single-pass cell. We chose this measurement because the energy meter had the widest range of errors among all the detectors used in our experiment. The energies and the powers of other pulses were estimated by operating the calibrating functions:

$$E_{ij} = \int P_{ij}\,dt = C_i \int F_{ij}\,dt, \tag{6}$$

where E, P, and F are the energy, the power, and the detected pulse profile, respectively; i corresponds to the pump or Stokes waves; and j corresponds to the input or output beam. The calibration constant C_p was obtained by Eq. (6) for the case of the output pump wave. We obtained C_s by solving the following equation:

$$C_s \int [F_{so}(t) - F_{si}(t)]dt = \frac{\omega_s}{\omega_p} C_p \int [F_{po}(t) - F_{pi}(t)]dt, \tag{7}$$

where absorption losses of these waves were neglected.

IV. Results

Examples of temporal pulse profiles obtained experimentally are shown in Fig. 3. Figure 3(a) presents profiles of pump and Stokes pulses at the entrance and Fig. 3(b) shows those at the exit after passing through the single-pass cell. By comparing Figs. 3(a) and 3(b), we see that the two pump pulses show a close resemblance to each other, except for the depleted portion. The increased depth of the dip in the pump pulse of Fig. 3(b) indicates that the two pulses experienced SRS in the transit of the single-pass cell.

Various sets of pulse profiles were acquired for numerical calculation. Some of them are shown in Fig. 4, where the initial powers are the same as indicated in Fig. 3(a). In Figs. 4(a), 4(b), and 4(c), different values of the gain coefficient 0.7 g_0, g_0, and 1.3 g_0 were given, respectively; g_0 is the value for $\Delta E_s' = \Delta E_s$. With the increase of the gain coefficient, ΔE_s and the Stokes peak power increased and the corresponding pump power was depleted. For the case of Fig. 4(b), the converted energy $\Delta E_s'$ agreed well with an experimentally obtained value of ΔE_s. Excellent agreement was also obtained on the temporal profiles.

In Fig. 5, g_0 is indicated as a function of the pressure of para-H_2. Gain coefficients obtained experimentally are averaged for some ten pulses and are plotted by solid circles with error bars. The solid curve represents gains calculated theoretically by Eq. (17), which appears in Appendix A. The value of $(\partial\sigma/\partial\Omega)$ required for the calculation is obtained from the anisotropic polarizability γ_{00} for the $S(0)$ transition of para-H_2. We adopted the value of γ_{00} reported by Midorikawa *et al.*[5] The value of Γ is given by the Raman linewidth,[18,19] which consists of the pressure-broadened width[20] and the diffusion-limited width.[18] As a result, the values of the gain coefficient obtained experimentally and the ones calculated theoretically show excellent agreement.

V. Discussion

In this section, we first discuss the advantage of the large-signal measurement in the transient limit.

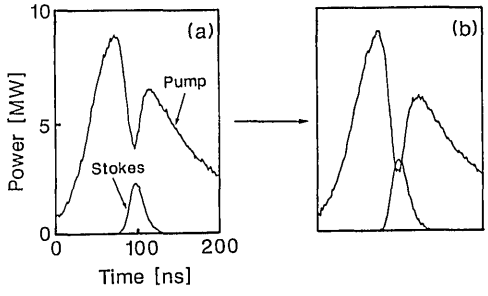

Fig. 3. Typical temporal profiles of pump and Stokes pulses obtained experimentally: (a) profiles of pulses before entering the single-pass cell, i.e., those of pulses emitted from a MPC. (b) profiles that experienced the amplification for the Stokes power and the depletion for the pump power through the single-pass cell.

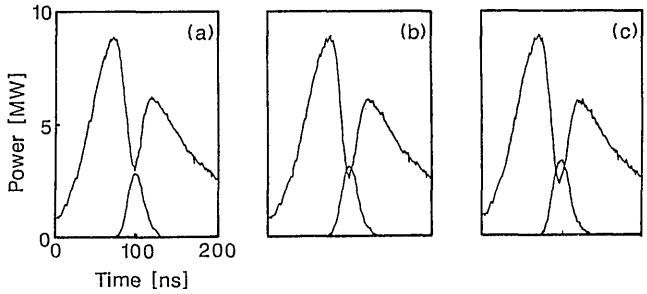

Fig. 4. Numerically calculated pump and Stokes pulse profiles. Temporal pulse profiles shown in Fig. 3(a) are used as the initial pump pulses. These profiles are compared with those indicated in Fig. 3(b). (a), (b), and (c) indicate the results when $g_0 \times 0.7$, g_0, and $g_0 \times 1.3$ are assumed as a plane-wave Raman Gain coefficient, respectively. The gain coefficient is g_0, which makes $\Delta E_s'$ equal to ΔE_s.

In the MPC that is operated below the saturation level, it is known that output Stokes energy varies in several orders of magnitude according to a slight fluctuation of pump energies. In addition to the change of peak powers, the instability of temporal and spatial profiles of pump pulses enhances such large variations of Stokes energies. In contrast, the large-signal measurement becomes more complex mathematically but simpler experimentally, because it is operated in the saturation region. In this experiment the whole pulse profiles were taken into account, so the error range was below ±10%. These errors are supposed to be caused by the energy meter, which has the largest margin of error ($\delta E/E \doteqdot 0.1$) among factors involved in the experiment.

Most of the ambiguities in the measurement of Raman gain diminished by use of a single-pass cell in place of a MPC. One problem left to be settled is the treatment of the transient effect, which effectively reduces the net gain. To solve this problem, we must measure the pulse profiles of both pump and Stokes pulses to analyze the transient response quantitatively. As a result of transient effect, the shape

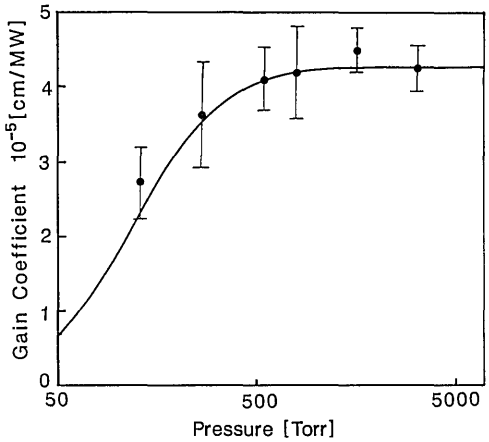

Fig. 5. Pressure dependence of the Raman gain coefficient of para-H_2. Values obtained experimentally are plotted with error bars. Theoretically calculated values are indicated by the solid curve.

of a Stokes pulse differs from that of a pump pulse. Stokes pulses are delayed to the pump pulses and their pulse width becomes narrower than that of the pump pulse. In the small-signal region the delay time of Stokes pulses increases, but the pulse width decreases with the increase of the Stokes power.[12,21] Transient effect can be neglected when the term Γt_p is sufficiently large, in which t_p is the pump-pulse width. Only when this requirement is satisfied can the Stokes power increase in the steady-state regime; this power is described by Eq. (18). In this sense, the analysis using Eq. (18) by Carlsten and Wenzel[6] and Uchida *et al.*[7] was inadequate for precise evaluation, because the transient effect was neglected. In the transient regime, the precise gain coefficient should be determined by the different expression from Eqs. (18) and (20); the expression has to involve the Stokes pulse shape, including the delay time to the pump pulse as carried out in this experiment. A comparison of temporal change of pump- and Stokes-pulse profiles is easier in the large-signal region than in the small-signal region.

As we mentioned previously, gain values obtained using a MPC were usually smaller by a factor of 0.7 than the theoretical value. In addition to the transient effect, possible causes of such a disagreement will be attributed to the following factors. First, there may be diffraction losses at the holes in the mirrors for multiple passes and uncertainties of the interaction volume or length in the beam-crossing configuration. The beam-crossing effect depends on crossing angles and the transverse distribution of intensities of beams. Although there are several hundred crossing points in a MPC and the temporal pulse width of a pumping CO_2 pulse with tail is wide enough to cross all the points, the effect of beam crossing has been ignored. Second, the reflectivity of mirrors in the MPC may be overestimated. When R indicates the reflectivity of MPC mirrors, ΔR indicates the error range of R and n indicates the number of reflections in the MPC; the range of error expands to $\pm n\Delta R R^{n-1}$. For example, when ΔR is estimated to be 1%, the total uncertainty of the transmittance of the MPC exceeds 20%. Finally, there may be an influence from a small amount of higher-order transverse modes of the pump beam and a slight difference in the mode-matching condition of pump and generated Stokes beams in the MPC.

From a viewpoint of the physical mechanism in SRRS, the gain coefficient of para-H_2 for a circularly polarized CO_2 laser is worth measuring because of its simple dynamic process. The successful agreement of this measurement should be attributed to this physical property. For precise measurement of the gain coefficient of SRS, the Raman process should be simple, so that there is no other competitive nonlinear optical effects, such as the generation of higher-order Stokes and anti-Stokes waves. The SRRS with the S(0) transition in para-H_2 pumped by a TEA–CO_2 laser meets these severe requirements. In this system, the description of the interaction between the electromagnetic waves and the molecule is given as the simplest way because only the rotational levels of $J = 0$ and 2 interact with the photon. Furthermore, in the SRRS process, four-wave mixing is controlled by the condition of the polarization of the pump wave.[22,23] With circularly polarized pump waves, the anti-Stokes wave is not generated because of the angular-momentum conservation in the SRRS process. The interaction length of a single-pass cell is too short for the generation of the second Stokes wave, which was found in a N_2-cooled Raman MPC.[24]

In conclusion, the plane-wave gain coefficient of SRRS in para-H_2 is determined precisely by measuring the energy conversion in a large-signal region. Obtained gain coefficients showed good agreement with the values led by the theoretical calculation, which is based on the polarizability anisotropy of para-H_2. The precise agreement was acquired by the carefully arranged experimental configuration and a numerical analysis of the Raman conversion process. The features of the method are that (1) single-transit measurement was adopted, (2) the pump and Stokes waves were provided by a multiple-pass Raman laser system, and (3) two beams were interacted in the large-signal region to treat the transient response of the Raman medium.

Appendix A. Coupled Equations in the Transient SRS Regime and the Plane-Wave Gain Coefficient

In this section, we introduce equations of pump and Stokes fields and the nonlinear vibration coupled by nonlinear polarization. The transverse-intensity distribution is treated in the limit of the TEM_{00} mode. The focusing points and the beam-waist sizes of the pump and Stokes beams are given independently to fit the equations to the experimental configurations.

When a photon density is large enough in the SRS process, the electromagnetic field and the vibrational motion of molecules can be treated by classical description. We follow the treatment given by Kaiser and Maier.[14] A set of differential equations for the electric fields and molecular system is prepared. It is coupled by nonlinear polarization. When the anti-Stokes wave and the second Stokes wave are neglected, the coupled equations are written as

$$\frac{n_p}{c}\frac{\partial E_p}{\partial t} + \frac{\partial E_p}{\partial z} = \frac{\pi i \omega_p}{n_p c} N \left(\frac{\partial \alpha}{\partial q}\right) q E_s - 1/2\, \alpha E_p, \tag{8a}$$

$$\frac{n_s}{c}\frac{\partial E_s}{\partial t} + \frac{\partial E_s}{\partial z} = \frac{\pi i \omega_s}{n_s c} N \left(\frac{\partial \alpha}{\partial q}\right) q^* E_p - 1/2\, \alpha E_s, \tag{8b}$$

$$\frac{\partial q}{\partial t} + \frac{\Gamma}{2} q = \frac{i}{4\omega_R m}\left(\frac{\partial \alpha}{\partial q}\right) E_p E_s^*, \tag{8c}$$

where E_p and E_s are the Fourier components of the electric fields corresponding to the pump and Stokes waves; q is the expectation value of the displacement in the molecular vibration; $(\partial\alpha/\partial q)$ is the derivative of the polarizability with respect to the normal coordinate, q; N is the number difference of molecules between the ground state and the excited state in a

unit volume; m is the reduced mass associated with the vibration; ω_p, ω_s, and ω_R are the angular frequencies of the pump and Stokes waves and the molecular vibration, respectively; n_p and n_s are the refractive indices of the medium for the pump and Stokes waves; and α is the power-absorption coefficient. For these three differential equations, we assume that the electric field consists of a sum of plane waves with slowly varying amplitude and phases. The backward SRS is ignored because the fairly intense Stokes probe pulse always propagates coincidently in the same direction as the pump wave in our experimental condition.

In Eq. (8c), the slowly varying envelope approximation and the assumption that $\Gamma \ll \omega_R$ are also applied. In the molecular system, because the number of molecules is large enough compared with that of the pump and the Stokes photon, the variation of the population difference Δ between the ground and the excited states can be neglected, even if the large-signal Raman interaction is applied. In the transient forward SRS regime, angular frequencies and wave numbers are restricted to the resonant case,

$$\omega_p - \omega_s = \omega_R, \tag{9a}$$

$$k_p - k_s = k_R. \tag{9b}$$

Without considering phases, we find that Eqs. (8a) and (8b) are expressed by the light intensity,

$$I = \frac{cn}{8\pi}|E|^2, \tag{10}$$

and Eq. (8c) is rewritten by the expression,

$$Q = N\sqrt{|q|^2}. \tag{11}$$

Then, Eqs. (8) are expressed as

$$\frac{1}{c}\frac{\partial I_s}{\partial t} + \frac{\partial I_s}{\partial z} = -\frac{\omega_p}{\omega_s} AQ\sqrt{I_p I_s}, \tag{12a}$$

$$\frac{1}{c}\frac{\partial I_s}{\partial t} + \frac{\partial I_s}{\partial z} = AQ\sqrt{I_p I_s}, \tag{12b}$$

$$\frac{dQ}{dt} + \frac{\Gamma}{2}Q = B\sqrt{I_p I_s}, \tag{12c}$$

where

$$A = 2\pi c\left(\frac{2m\omega_R}{\hbar\omega_p\omega_s}\frac{d\sigma}{d\Omega}\right)^{1/2}, \tag{13a}$$

$$B = \frac{2\pi cN}{\omega_s}\left(\frac{2}{\hbar\omega_p\omega_s\omega_R m}\frac{d\sigma}{d\Omega}\right)^{1/2}, \tag{13b}$$

and where the relation between $(\partial\alpha/\partial q)$ and the total spontaneous differential-scattering cross section $(d\sigma/d\Omega)$ are written as

$$\frac{d\sigma}{d\Omega} = \frac{\omega_s{}^3\omega_p\hbar}{2m\omega_R c^4}\left(\frac{\partial\alpha}{\partial q}\right)^2. \tag{14}$$

In the infrared region, the refraction indices n_p and n_s can be approximated to be 1.

For the steady-state calculation, an approximation that

$$\frac{\partial Q}{\partial t} \ll \frac{\Gamma}{2}Q \tag{15}$$

is applied, where vibrations in the molecule are heavily damped. The following equations are thus obtained:

$$\frac{1}{c}\frac{\partial I_p}{\partial t} + \frac{\partial I_p}{\partial z} = -\frac{\omega_p}{\omega_s} gI_p I_s, \tag{16a}$$

$$\frac{1}{c}\frac{\partial I_s}{\partial t} + \frac{\partial I_p}{\partial z} = gI_p Is, \tag{16b}$$

where g is the plane-wave Raman gain coefficient in the steady-state regime and is written as

$$g = \frac{16\pi^2 c^2 N}{\hbar\omega_s{}^2\omega_p\Gamma}\frac{d\sigma}{d\Omega}. \tag{17}$$

Assuming that I_p has a constant value, we find that the solution of Eq. (16b) results in the following equation:

$$I_s = I_{s0}\exp(gI_p l). \tag{18}$$

In the estimation using the above equations, the transverse mode of the pump and Stokes beams is assumed to be the TEM_{00} mode. The spatial distribution of the light intensity is indicated as a Gaussian curve,[15] which is expressed as

$$I(z, r, t) = \frac{2P(z, t)}{\pi W(z)^2}\exp\left[-2\left(\frac{r}{W(z)}\right)^2\right], \tag{19}$$

where $P(z, t)$ is the power of light at a point z. Substituting $I(z, r, t)$ into Eqs. (16), we can express pump and Stokes waves by the power of them, i.e.,

$$\frac{dP_p}{dZ} = -\frac{\omega_p}{\omega_s}\frac{2gP_pP_s}{\pi[W_p(z)^2 + W_s(z)^2]}, \tag{20a}$$

$$\frac{dP_s}{dZ} = \frac{2gP_pP_s}{\pi[W_p(z)^2 + W_s(z)^2]}, \tag{20b}$$

where a Galilei transformation is operated with the relation that $Z = z + (c/n)t$. This formalism is also applied to the set of differential equations in the transient regime. According to Eq. (12c), the spatial distribution of Q is supposed to be related to $\sqrt{I_p I_s}$. The spatial distribution of Q is then written as

$$Q = V\left\{\frac{2}{\pi W_v}\exp\left[-2\left(\frac{r}{W_v}\right)^2\right]\right\}^{1/2}, \tag{21}$$

where

$$\frac{1}{W_v(z)^2} = \frac{1}{W_p(z)^2} + \frac{1}{W_s(z)^2}, \tag{22}$$

and V reflects the spatially integrated value of Q. Then the Raman conversion equations are developed to include the spatial distribution of the TEM_{00} mode. The developed equations shown in Eqs. (1) are obtained by substituting Eqs. (19) and (21) into Eqs. (12).

The authors acknowledge discussions with and instructive advice from Katsumi Midorikawa. They also acknowledge the technical assistance of and operation of the simulation codes by Takeshi Shimada and Atsunori Kitazawa.

References

1. R. L. Byer, "A 16-μm source for laser isotope enrichment," IEEE J. Quantum Electron. **QE-12,** 732–733 (1976).
2. P. Rabinowitz, A. Stein, R. Brickman, and A. Kaldor, "Stimulated rotational Raman scattering from para-H2 pumped by a CO_2 TEA laser," Opt. Lett. **3,** 147–148 (1978).
3. P. Rabinowitz, A. Stein, R. Brickman, and A. Kaldor, "Efficient tunable H_2 Raman laser," Appl. Phys. Lett. **35,** 739–741 (1979).
4. K. Midorikawa, H. Tashiro, Y. Aoki, K. Ohashi, K. Nagasaka, E. Toyada, and S. Namba, "Output performance of a liquid-N_2-cooled, para-H_2 Raman laser," J. Appl. Phys. **57,** 1504–1508 (1985).
5. K. Midorikawa, H. Tashiro, Y. Aoki, K. Nagasaka, K. Toyoda, and S. Namba, "Room-temperature operation of a para-H_2 rotational Raman laser," Appl. Phys. Lett. **47,** 1033–1035 (1985).
6. J. L. Carlsten and R. G. Wenzel, "Stimulated rotational Raman scattering in CO_2-pumped para-H2," IEEE J. Quantum Electron. **QE-19,** 1407–1413 (1983).
7. M. Uchida, K. Nagasaka, and H. Tashiro, "Enhancement of Stokes conversion by diode-laser injection in a para-H_2 Raman laser," Opt. Lett. **14,** 1350–1352 (1989).
8. N. Bloembergen, "The stimulated Raman effect," Am. J. Phys. **35,** 989–1023 (1967).
9. W. R. Trutna and R. L. Byer, "Multiple-pass Raman gain cell," Appl. Opt. **19,** 301–312 (1980).
10. B. Perry, R. O. Brickman, A. Stein, E. B. Treacy, and P. Rabinowitz, "Controllable pulse compression in a multiple-pass cell Raman laser," Opt. Lett. **5,** 288–290 (1980).
11. E. J. Corat, V. J. T. Airoldi, S. L. Scolari, and C. C. Ghizoni. "Gain measurement in stimulated rotational Raman scattering in para hydrogen," Opt. Lett. **11,** 368–370 (1986).
12. R. L. Carman, F. Shimizu, C. S. Wang, and N. Bloembergen, "Theory of Stokes pulse shapes in transient stimulated Raman scattering," Phys. Rev. A **2,** 60–72 (1970).
13. M. D. Duncan, R. Mahon, L. L. Tankersley, and J. Reintjes, "Transient stimulated Raman amplification in hydrogen," J. Opt. Soc. Am. **5,** 37–52 (1988).
14. W. Kaiser and M. Maier, "Stimulated Rayleigh, Brillouin and Raman spectroscopy," in *Laser Handbook,* F. T. Arecchi and E. O. Schulz-Dubois, eds. (North-Holland, Amsterdam, 1972), pp. 1078–1150.
15. A. E. Siegman, "Physical properties of Gaussian beams," in *Lasers* (University Science Books, Mill Valley, Calif., 1986).
16. H. Tashiro, K. Midorikawa, K. Nagasaka, K. Toyoda, and S. Namba, "A CO_2-laser-pumped para-H2 Raman laser," Rev. Laser Eng. **13,** 292–304 (1985).
17. M. Suzuki and H. Tashiro, "Transverse-mode selection in a para-H_2 Raman laser with multiple reflection passes," J. Opt. Soc. Am. B. **8,** 1686–1691 (1991).
18. A. Owyoung, "High-resolution cw stimulated Raman spectroscopy in molecular hydrogen," Opt. Lett. **2,** 91–93 (1978).
19. J. L. Gersten and H. M. Foley, "Combined Doppler and collision broadening," J. Opt. Soc. Am. **58,** 933–937 (1968).
20. K. D. Van Den Hout, P. W. Hermans, E. Mazur, and H. F. P. Knaap, "The broadening and shift of the rotational Raman lines for hydrogen isotopes at low temperature," Physica (Utrecht) A **104,** 509–547 (1980).
21. T. Higashii, A. Tsunemi, K. Nagasaka, K. Midorikawa, and H. Tashiro, "Short-pulse generation in the transient Raman regime with a parahydrogen Raman laser," Jpn. J. Appl. Phys. **29,** 1454–1458 (1990).
22. R. W. Mink, E. E. Hagenlocker, and W. G. Rado, "Stimulated pure rotational Raman scattering in deuterium," Phys. Rev. Lett. **17,** 229–231 (1966).
23. R. Holmes and A. Flusberg, "Rotationally invariant theory of stimulated Raman scattering," Phys. Rev. A **37,** 1588–1596 (1988).
24. H. Tashiro, K. Midorikawa, Y. Aoki, K. Nagasaka, K. Toyada, and S. Namba, "Observation of the second Stokes wave in a para-hydrogen Raman laser," Opt. Lett. **10,** 80–82 (1985).